Astronomy & Astrophysics manuscript no. fuentes-carrera˙kar302
February 5, 2008
© ESO 2008

arXiv:astro-ph/0701878v1 30 Jan 2007

Kinematics and dynamics of the M51-type galaxy pair NGC 3893/96 (KPG 302)

I. Fuentes-Carrera[1⋆] M. Rosado[2], P. Amram[3], H.Salo[4], and E. Laurikainen[4]

[1] Instituto de Astronomía, Geofísica e Ciencias Atmosféricas, Universidade de São Paulo, Rua do Matão 1226-Cidade Universitária, 05508-900 São Paulo SP, Brazil
e-mail: isaura@astro.iag.usp.br,isaura.fuentes@obspm.fr
[2] Instituto de Astronomía, Universidad Nacional Autónoma de México (UNAM), Apdo. Postal 70-264, 04510, México, D.F., México
e-mail: margarit@astroscu.unam.mx
[3] Laboratoire d'Astrophysique de Marseille, 2 Place Le Verrier, Marseille Cedex 4, France
e-mail: philippe.amram@oamp.fr
[4] Department of Physical Sciences, Division of Astronomy, University of Oulu, FIN-90570, Oulu, Finland
e-mail: heikki.salo@oulu.fi,eija.laurikainen@oulu.fi

Received . . . . . ; accepted . . . . . .

ABSTRACT

Aims. We study the kinematics and dynamics of the M51-type interacting galaxy pair KPG 302 (NGC 3893/96). We analyse the perturbations induced by the encounter on each member of the pair, as well as the distribution of the dark matter (DM) halo of the main galaxy in order to explore possible differences between DM halos of "isolated" galaxies and those of galaxies belonging to a pair.
Methods. The velocity field of each galaxy was obtained using scanning Fabry-Perot interferometry. A two-dimensional kinematic and dynamical analysis of each galaxy and the pair as a whole is done emphasizing the contribution of circular and non-circular velocities. Non-circular motions can be traced on the rotation curves of each galaxy allowing us to differentiate between motions associated to particular features and motions that reflect the global mass distribution of the galaxy. For the main galaxy of the pair, NGC 3893, optical kinematic information is complemented with HI observations from the literature to build a multi-wavelength rotation curve. We try to fit this curve with a mass-distribution model using different DM halos.
Results. Non-circular motions are detected on the velocity fields of both galaxies. These motions can be associated to perturbations due to the encounter and in the case of the main galaxy, to the presence of structure such as spiral arms. We find that the multi-wavelength rotation curve of NGC 3893, "cleaned" from the effect of non-circular motions, cannot be fitted neither by a pseudo-isothermal nor by a NFW DM halo.

Key words. galaxies: interactions — galaxies: kinematics and dynamics — galaxies: individual (NGC 3893, NGC 3896) — galaxies: spiral — galaxies: halos

1. Introduction

The difference between the mass distribution implied by the luminosity of a disc galaxy and the distribution of mass implied by the rotation velocities offers strong evidence that disc galaxies are embedded in extended halos of dark matter (Sofue & Rubin 2001 and references there-in). Detailed knowledge of dark matter (DM) haloes around galaxies holds important clues to the physics of galaxy formation and evolution and is an essential ingredient for any model aiming to link the observable Universe with cosmological theories. In practice, realistic DM haloes are neither static nor spherically symmetric (Knebe, Gill & Gibson 2004) and it is still unknown if their structure and distribution is intrinsically related to the environment of their galaxies. The question remains if there exists an intrinsic difference between the DM halo of an "isolated" galaxy, the DM halo of a galaxy belonging to a pair or that of a galaxy that is part of a larger group such as a compact group or a cluster.

In this sense, rotation curves (RCs) are a powerful tool to study the distribution of matter (both baryonic and non-baryonic) in interacting disc galaxies. For a description of the classical method for studying mass distribution see Blais-Ouellette, Amram & Carignan (2001) and references there-in. RCs also allow us to determine the maximum rotation velocity of a galaxy and thus infer the total mass within a certain radius using methods such as that of Lequeux (1983). Nevertheless, care must be taken when using kinematic information from interacting galaxies since they are subject to kinematical perturbations that may affect the correct determination of a RC that actually traces the global mass distribution of the galaxy. For this reason, 3D spectroscopy observations are required to separate circular from non-circular motions in the velocity field of a galaxy and its rotation curve as shown in Fuentes-Carrera et al. (2004).

Send offprint requests to: I. Fuentes-Carrera
⋆ Presently at the Observatoire de Paris-Meudon

In this work, we present scanning Fabry-Perot observations of the M51-type interacting galaxy pair NGC 3893/96 (KPG 302). Section 2 present the scanning Fabry-Perot (FP) observations and data reductions. Section 3 introduces the pair of galaxies KPG 302 (NGC 3893/96). In section 4 we present the kinematic information derived from the F-P observations. Section 5 presents the dynamical analysis of both galaxies, mass estimates as well as the mass distribution for NGC 3893. The discussion and conclusions are presented in sections 6 and 7, respectively.

2. Observations and Data Reductions

Observations of NGC 3893/96 (KPG 302) were done at the 2.1m telescope at the OAN-SPM (México) using the scanning Fabry-Perot interferometer PUMA (Rosado et al. 1995). PUMA is a focal reducer built at the Instituto de Astronomía-UNAM used to make direct images and Fabry-Perot (FP) interferometry of extended emission sources (field of view 10′). The FP used is an ET-50 (Queensgate Instruments) with a servostabilization system having a free spectral range of 19.95 $\AA$ (912 $km\ s^{-1}$) at $H\alpha$. Its finesse ($\sim$ 24) leads to a sampling spectral resolution of 0.41 $\AA$ (19.0 $km\ s^{-1}$) achieved by scanning the interferometer free spectral range through 48 different channels. A 1024×1024 Tektronix CCD detector with a resolution of 0.58 $''/pixel$ was used. We used a 2×2 binning in order to enhance the signal. The final spatial sampling equals 1.16 $''/pixel$. In order to isolate the redshifted $H\alpha$ ($\lambda_{at\ rest} = 6562.73\ \AA$) emission of the galaxies, we used an interference filter centered at 6584 $\AA$ with a $FWHM$ of 10$\AA$. To average the sky variations during the exposure, we got two data cubes with an exposure time of 48 minutes each (60 s per channel). These data cubes were co-added leading to a total exposure time of 96 minutes. For the calibration we used a H lamp whose 6562.78 $\AA$ line was close to the redshifted nebular wavelength. Two calibration cubes were obtained at the beginning and at the end of the galaxy observation to check the metrology.

Data reduction and analysis were done using mainly the ADHOCw[1] and CIGALE softwares (LeCoarer et al. 1993). Standard corrections (cosmic rays removal, bias subtraction, flat-fielding,...) were done on each cube. Once the object cubes were co-added, the night sky continuum and 6577.3$\AA$ OH sky line were subtracted. A spectral Gaussian smoothing ($\sigma = 57\ km\ s^{-1}$) was also performed. Once the spectral smoothing was done, the calibration in wavelength was fixed for each profile at each pixel using the calibration cube. The Fabry-Perot scanning process allows us to obtain a flux value at pixel level for each of the 48 scanning steps. The intensity profile found along the scanning process contains information about the monochromatic emission ($H\alpha$) and the continuum emission of the object. The continuum image computation was done considering the mean of the 3 lowest intensities of the 48 channels cube. For the monochromatic image, the $H\alpha$ line intensity was obtained by integrating the monochromatic profile in each pixel. The velocity maps were computed using the barycenter of the $H\alpha$ profile peaks at each pixel. In order to get a sufficient signal-to-noise ratio on the outer parts of each galaxy, we performed three spatial Gaussian smoothings ($\sigma = 2.36,\ 3.54,\ 4.72\ ''$) on the resulting calibrated cube. A variable-resolution radial velocity map was built using high spatial resolution (less spatially-smoothed pixels) for regions with originally higher signal-to-noise ratio.

[1] *http://www.oamp.fr/adhoc/adhocw.htm* developed by J. Boulesteix

3. NGC 3893 and NGC 3896

NGC 3893/96 is an interacting galaxy pair with number 302 in the Catalogue of Isolated Pairs of Galaxies in the Northern Hemisphere (KPG, Karachentsev 1972). Morphologically it resembles M51 (NGC 5194/95) since it is composed of a main spiral galaxy and a considerably smaller companion. KPG 302 is situated in the Ursa Major cluster. With only 79 members, this cluster is poorly defined with a velocity dispersion of only 148 $km\ s^{-1}$ and a virial radius of 880 kpc (Tully et al. 1996). It contains essentially only late-type galaxies distributed with no particular concentration toward the center. Given the isolation criteria **used in the KPG** and the nature of the cluster, it is possible that the DM halo (or haloes) of the galaxies in the pair are isolated from those of the cluster.

NGC 3893 is a grand-design spiral similar to NGC 5194 in M51 (Figure 1a). It has been classified as SABc in LEDA database, and as SAB(rs)c in NED[2] database and in the RC3 (de Vaucouleurs et al. 1991). However, Hernández-Toledo & Puerari (2001) classify it as a non-barred galaxy without any inner ring. HI observations (Verheijen & Sancisi 2001), show that this galaxy is slightly warped in its outer parts -both in its HI distribution and its HI kinematics. Its companion, NGC 3896, appears to be an intermediate type galaxy between and S0 and a spiral, having also a bar. It shows extended $H\alpha$ emission. NGC 3893 shows no color excess, whereas NGC 3896 has predominantly blue $B - V$ color in the central parts of the galaxy (Laurikainen, Salo & Aparicio 1998; Hernández-Toledo & Puerari 2001).

The star-formation rate (SFR) of each member of the pair was derived by James et al. (2004). These authors found a value of 5.62 $M_\odot\ yr^{-1}$ for NGC 3893 and a value of 0.14 $M_\odot\ yr^{-1}$ for its companion. NGC 3893 was also part of a dynamical analysis of high surface spiral galaxies using long-slit observations and numerical modelling in order to quantify the luminous-to-dark matter ratio inside their optical radii (Kranz, Slyz & Rix 2003). According to these authors, NGC 3893 has a massive stellar disc which dominates the dynamics of the central regions with a disc mass of 2.32×10^{10} solar masses. They infer the location of the corotation resonance of this galaxy at $5.5 \pm 0.5\ kpc$. Though optical images of this pair do not show an apparent connection between the two galaxies, radio images by Verheijen & Sancisi (2001) show extended HI emission encompassing both galaxies (small panel in Figure 1). This common HI envelope is elongated from SE to NW, parallel to the line that joins the nuclei of both galaxies. HI isophotes also show what could be considered as a broad arm going from NGC 3893 to NGC 3896. Table 1 lists the main parameters of each galaxy.

[2] The NASA/IPAC Extragalactic Database (NED) is operated by the Jet Propulsion Laboratory, California Institute of Technology, under contract with the National Aeronautics and Space Administration.

4. Kinematic results

4.1. Monochromatic Images

Figure 1b displays the monochromatic $H\alpha$ image of the pair. Knotty HII regions lie along the spiral arms of NGC 3893. Though they mainly follow the two main arms, they also outline small segments of fainter and less pronounced flocculent arms. Intense HII regions are seen on the east side of the galaxy along the western spiral arm. A very bright HII region is seen in the central parts of the galaxy.

For NGC 3896, important $H\alpha$ emission is seen within the inner 13.9 $''$ (1.3 kpc) southeast of the center of the galaxy. This emission displays two maxima that form a rather elongated region (left panel in Figure 1b). The northern parts of the galaxy show weak diffuse emission. This type of emission is also seen on the western side of the galaxy. These sides are closer to NGC 3893.

4.2. Velocity Fields

The upper panel in Figure 2 shows the velocity field of NGC 3893. It is a smooth and regular field; the isovelocities show no significant distortions. Although the galaxy has an elongated inner structure in the monochromatic image (see Figure 1), the central parts of the galaxy show no kinematic signatures that could be associated to the presence of a nuclear bar. The minor kinematic axis is almost perpendicular to the main axis of the galaxy - outlined by isovelocities with 955 $km\ s^{-1}$. Small wiggles seen along these isovelocities could be a signature of an inner ring, similar to that shown by the simulations by Salo et al. (1999) of IC4214. The velocity field is symmetrical with respect to the kinematical minor axis. Locally, minor irregularities are seen in the distribution of radial velocities, especially along the spiral arms of the galaxy. These might be associated to the passage of gas through the spiral density wave. For NGC 3896, the velocity field is very perturbed displaying a mild velocity gradient from the SE to the NW (upper panel in Figure 3). Isovelocities are very patchy and crooked.

4.3. Rotation Curves

In the case of early-stage interactions, the inner parts of galaxies are not strongly perturbed, velocity fields are still smooth and symmetrical resulting in symmetric and low-scattered rotation curves (RCs) up to a certain radius bf (Fuentes-Carrera et al. 2004). With this assumption in mind, the RC of each galaxy was computed considering different values for the kinematical parameters involved in order to obtain a symmetric curve in the inner parts of the galaxy and to minimize scatter on each side of the curve. The rotation curves are sampled with bins of 2 pixels ($\sim 2.3''$). Error bars give the dispersion of the rotation velocities computed for all the pixels found inside each elliptical ring defined by the successive bins. This approach is described in more detail in Fuentes-Carrera et al. (2004) and Garrido et al. (2005).

4.3.1. NGC 3893

The RC of NGC 3893 was computed considering points on the velocity field within an angular sector of 32° on each side of the galaxy's $P.A.$ The kinematic center used to compute the rotation curve matches the photometric center from the PUMA continuum image within $1''$. The most symmetrical, smooth and less-scattered RC was derived using the following set of values: $P.A. = (340 \pm 10)°$, $i = (45 \pm 3)°$ and $V_{sys} = (962 \pm 5)\ km\ s^{-1}$. These are presented in Table 1 along with values obtained in previous works. The RC superposing both the approaching and receding sides is shown in the lower panel in Figure 2. Globally the RC of NGC 3893 is symmetric up to the last $H\alpha$ emission point at $85''$ (7.55 kpc). Both sides of the curve display oscillations of about 10 $km\ s^{-1}$. The maximum rotation velocity is $(197 \pm 10)\ km\ s^{-1}$ and is reached at $69''$ (6.1 kpc). Our RC is very similar to that derived by Garrido et al. (2002) using FP observations. In order to compare with the results derived by Kranz, Slyz & Rix (2003), a long-slit was simulated by considering radial velocities on the velocity field within a sector of 1.5° on each side of the slit position angle. The values of the kinematic parameters were equal to those used by these authors. These "long-slit" RCs show the same increasing behavior and oscillations as those found by Kranz, Slyz & Rix (2003).

4.3.2. NGC 3896

Though the velocity field of this galaxy is very perturbed, we were still able to derive a RC reflecting the circular motions of the southwestern side of the galaxy (approaching side). The following set of values were used: $P.A. = (294 \pm 5)°$, $i = (49 \pm 3)°$ and $V_{sys} = (920.50 \pm 5)\ km\ s^{-1}$, considering an angular sector of 42° on each side of the galaxy's $P.A.$. These values along with values from previous works are presented in Table 1. The lower panel in Figure 3 shows the RC derived for this galaxy superposing both the approaching and receding sides. Globally the curve displays an increasing behavior up to the last emission point at $17.5''$ (1.5 kpc) where the velocity equals 48 $km\ s^{-1}$. Rather small velocity values appear near the center of the galaxy, within $4.2''$ (0.4 kpc).

4.4. Non-circular motions

Two dimensional kinematic fields of disc galaxies portray the motion of the gas all over the galaxy enabling us to match these motions with different morphological structures. One can determine to which extent the gas is following circular motion around the center of the galaxy and to which extent there are important contributions from non-circular velocities (radial, azimuthal and vertical) due to the presence of these structures or external perturbations. For NGC 3893, we analysed the influence of morphological features on the kinematics of the gas. This was done by comparing the monochromatic image with each side of the RC (Figure 4). Through this comparison we were able to differentiate points in the RC associated to circular motions of the gas -associated with the global mass distribution of the galaxy- from non-circular motions -associated to the response of the gas to local morphological features.

5. Dynamical Analysis

5.1. Mass Estimates through Rotation Curves

The $H\alpha$ kinematic information from our FP observations of NGC 3893 was complemented with HI synthesis observations by Verheijen & Sancisi (2001). In order to match both curves, we considered the averaged optical rotation curve which was derived using the same kinematic parameters as those used for the HI RC (these values do not differ much from the values we used for the optical RC - see Table 1). The superposed curves are shown in Figure 5. Both curves superpose smoothly except for the external parts of the optical RC ($R \geq 60''$) which appear to be more perturbed. The HI RC also displays a decreasing behaviour for $R \geq 175''$ and up to the last HI emission point at $R = 245''$ (21.76 kpc). Verheijen & Sancisi (2001) mention that the determination of the HI rotation curve beyond $120''$ is uncertain because of the tidal interaction with NGC 3896. We shall set this radius as our limit for the computation of the mass through the RC of NGC 3893. Using this composite rotation curve, a range of possible masses was computed using the method proposed by Lequeux (1983) according to which the total mass of a galaxy within a radius R lies between 0.6 (in the case of a disc-like mass distribution) and 1.0 $\times (RV^2(R)/G)$ (in the case of a spheroidal mass distribution). As a first estimate, we considered the maximum rotation velocity (190 $km\ s^{-1}$) given by both the optical and radio RCs to estimate the mass within $R = 120'' = 10.8\ kpc = 0.99\ D_{25}/2$. The range of masses within this radius is given by 0.50 to $0.84 \times 10^{11} M_{\odot}$. In order to derive the mass of NGC 3896, we considered the last emission point on the approaching side of the curve which shows the maximum amplitude of that curve. This value equals 48 $km\ s^{-1}$ at $R = 17.5'' = 1.5\ kpc = 0.4\ D_{25}/2$. The range of masses within this radius is from 4.78 to $7.97 \times 10^8 M_{\odot}$. The mass ratio of the galaxies was computed based on the NIR luminosities, calculated from the K_s-magnitudes taken from 2MASS (Skrutskie et al. 2006). These luminosities for NGC 3893/96 lead to the mass ratio of 0.031. On the other hand, the mass ratio derived from the RC of each galaxy within 0.4 $D_{25}/2$ falls around 0.0255. These values are fairly similar, particularly if considering the uncertainty of the mass-to-light ratio. This fact strengthens the reliability of the mass estimates based on the rotation curves.

5.2. Mass Distribution

In order to study the mass distribution in NGC 3893 we used the mass model from Blais-Ouellette, Amram & Carignan (2001). This model uses both the light distribution of the galaxy and a theoretical dark halo profile to compute a RC that best fits the observed one. The mass-to-light ratio of the disc $(M/L)_{disk}$) as well as the properties of the dark matter, characteristic density (ρ_0) and radius (R_0), are free parameters. We used a DM halo described by a pseudo-isothermal sphere (Begeman 1987) and a Navarro, Frenk & White (NFW) profile (Navarro, Frenk & White 1996) in order to fit the multi-wavelength RC of NGC 3893. Optical photometry in the I band was taken from Hernández-Toledo & Puerari (2001) and the HI superficial distribution from Verheijen & Sancisi (2001). Making use of the possibility to disentangle circular from non-circular velocities in the optical RC, our multi-wavelength RC was "cleaned" from points associated to non-circular motions (see section 4.4) and to the warp in the outer parts of the HI disc. We removed points in the optical part of the observed RC between $15''$-$20''$, $22''$-$32''$ and at R> $75''$ (see Figure 5). Only points from the HI rotation curve were taken into account after $75''$ and up to $120''$ considering the fact that the RC in HI is uncertain beyond this radius.

Figure 6 shows different fits for this multi-wavelength RC: a pseudo-isothermal DM halo with non-maximal disc (*top left*), a pseudo-isothermal DM halo with a maximal disc (*top right*), a NFW halo with non-maximal disc (*bottom left*) and a NFW halo with a maximal disc (*bottom left*). Table 2 displays the mass model parameters used in each case. We used the definition of Sackett (1997) for the "maximal disc" which is taken to be a galactic disc such that $85\% \pm 10\%$ of the total rotational support of a galaxy at a radius $2.2 xscaleradius$ is contributed by the stellar disc mass component. For NGC 3893, this radius corresponds to 1.80 kpc (Kranz, Slyz & Rix 2003). The best fit ($\chi^2 = 1.34$) is obtained using a pseudo-isothermal halo with a non-maximal disc leading to $(M/L)_{disc} = 0.94$ in the I band, yet it misses the last two points of the RC. The fit with a NFW halo and a non-maximal disc gives $(M/L)_{disc} = 0.24$ ($\chi^2 = 1.43$), also missing the two outermost points of the RC. Both a pseudo-isothermal and NFW halo with a maximal disc give larger values of $(M/L)_{disc}$ (1.25 in both cases) and also larger χ^2 values (1.53 and 3.11, respectively). They also miss both outer and inner points on the RC.

In order to evaluate the effect of non-circular motions on the fits, we fitted the above mass models including the points associated to non-circular motions to the multi-wavelength RC. The fits can be seen in Figure 7. The values for the mass model parameters are shown in Table 2. These fits are less precise. In all cases, the mass-to-luminosity ratio using the maximal disc assumption is larger than that obtained by Kranz, Slyz & Rix (2003) ($(M/L)_{disc} = 0.56$ -in both K and I bands). We must take into account the fact that Kranz, Slyz & Rix (2003) only fit the optical part of the RC derived with long-slit spectroscopy. For the sake of comparison, we fitted our Hα RC (with and without points associated to non-circular motions) using the value for $(M/L)_{disc}$ derived by these authors. Results are shown in Figure 8 and Table 2. Fits are very good for both the pseudo-isothermal and the NFW halo, nevertheless $(M/L)_{disc} = 0.56$ does not render the disc maximal. Finally we also fitted these mass models to the HI RC without points at $R > 120''$ where tidal effects might affect the correct determination of the RC. Figure 9 and Table 2 show the resulting parameters of the fits. The fit using the NFW halo misses the inner most point of the curve and is rather inaccurate ($\chi^2 = 3.17$). The fit using the pseudo-isothermal halo misses the middle point of the curve, yet $\chi^2 = 1.32$ -which is on the of the lowest values found for all fits presented. Nevertheless it should be noticed that for both haloes, the $(M/L)_{disc} > 1.7$ which is larger than the value found with the multi-wavelength RC. This highlights the importance of the multi-wavelength approach for the mass model.

6. Discussion

The fact that no model fits the last point in the multi-wavelength RC of NGC 3893 "cleaned" from the effects of non-circular motions can be explained either by a truncated halo for this galaxy or by the existence of a common halo for both galaxies. Since the derived mass of the NGC 3896 is small, then it most probably resides inside the halo of NGC 3893 and both galaxies share a single halo. Nevertheless this halo would have a different distribution than that of an isolated galaxy. When considering an isothermal halo and the HI curve, the $(M/L)_{disk}$ that best fits this curve is much higher than the M/L found for the multi-wavelength curve. In general, the information on the inner parts of the galaxy given by the optical observations imposes an $(M/L)_{disk} \leq 1$ which would imply the presence of a disc with an important population of young stars -which is not the case given the $B-V$ value derived by Hernández-Toledo & Puerari (2001). This supports the idea that the structure of the DM halo of this pair differs from that of a single disc galaxy. As shown by Laurikainen & Salo (2001), in general M51-type pairs companions have extremely large bulge sizes relative to their disc scale-lengths. Consequently, the bulge-to-disc luminosity ratios for the companions were also generally larger than known for any of the Hubble types of normal galaxy. This is the case for NGC 3896 whose RC displays almost solid body rotation up to the last emission point.

7. Conclusions

We have presented the kinematic and dynamical analysis of the M51-type galaxy pair, KPG 302 (NGC 3893/96). NGC 3893 is a grand-design spiral with a regular velocity field that displays no major distortions. The companion, NGC 3896 displays on-going star formation which was probably triggered by the interaction with the main galaxy. This galaxy displays important non-circular motions in localized regions, especially on the side of the galaxy which is closer to the companion. The total mass of each galaxy was derived from the RC. The optical RC of NGC 3893 was matched with the existing HI curve in order to determine the distribution of the luminous and dark matter. This multi-wavelength rotation curve was analysed in the light of the 3D observations in order to differentiate the contribution of non-circular motions, associated to particular features, and the contribution of circular motions, which reflect the mass distribution of the galaxy. No "classical" DM halo fits the observed rotation curve which could imply a different mass distribution for the DM halo of M51-type binary galaxies.

Acknowledgements. We wish to thank the staff of the Observatorio Astronómico Naconal (OAN-SPM) for their support during PUMA data acquisition. We also thank C. Carignan for letting us use his mass model. I.F.-C. thanks the financial support of FAPESP and CONACYT grants no.03/01625-2 and no.121551 -respectively. M.R. acknowledges financial support from grants 46054-F from CONACYT and IN100606 from DGAPA-UNAM. H.S. and E.L. acknowledge the support from the Academy of Finland. We acknowledge the usage of the HyperLeda database (http://leda.univ-lyon1.fr), the NASA/IPAC Extragalactic Database (NED) and the Two Micron All Sky Survey.

References

Begeman, K.G. 1987, PhD thesis, Gronigen University
Blais-Ouellette, S., Amram, P. & Carignan, C. 2001, AJ, 121, 1952
Fuentes-Carrera, I., Rosado, M., Amram, P., Dultzin-Hacyan, D., Bernal,A., Salo, H., Laurikainen, E., Cruz-González, I., Ambrocio-Cruz, P. & Le Coarer, E. 2004, A&A, 415, 451
Garrido, O., Marcelin, M., Amram, P. & Boulesteix, J. 2002, A&A, 387, 812
Garrido, O., Marcelin, M., Amram, P., Balkowski, C. & Boulesteix, J. 2005, MNRAS, 362, 127
Hernández-Toledo, H. & Puerari, I. 2001, A&A, 379, 54
James, P.A., Shane, N.S., Beckman, J.E., Cardwell, A., Collins, C.A., Etherton, J., de Jong, R.S., Fathi, K., Knapen, J.H., Peletier, R.F., Percival, S.M., Pollacco, D.L., Seigar, M.S., Stedman, S., Steele, I.A. 2004, A&A, 414, 23
Karachentsev, I.D. 1972, Catalogue of isolated pairs of galaxies in the northern hemisphere, Soobshch.Spets.Astrofiz.Obs, 7, 1
Knebe, A., Gill, S.P.D. & Gibson, B.K. 2004, PASA, 21, 216
Kranz, T., Slyz, A. & Rix, H.-W. 2003, ApJ, 586, 143
Laurikainen, E., Salo, H. & Aparicio, A. 1998, A&ASupp.Ser., 129, 517
Laurikainen, E. & Salo, H. 2001, MNRAS, 324, 685
Le Coarer, E., Rosado, M., Georgelin, Y., Viale, A. & Goldes, G. 1993, A&A, 280, 365
Lequeux, J. 1983, A&A, 125, 394
Navarro,J.F., Frenk,C.S. & White,S.D.M. 1996, ApJ, 462, 563
Pasha,I.I. & Smirnov,M.A. 1982, Ap&SS, 86, 215
Rosado, M., Langarica, R., Bernal, A., Cobos, F., Garfias, F., Gutierrez, L., Tejada, C., Tinoco, S. & Le Coarer, E. 1995, RevMexAA (Serie de Conferencias), 03, 263
Sackett, P.D. 1997, ApJ, 483, 103
Salo, H., Rautiainen, P., Buta, R., Purcell, G.B., Cobb, M.L., Crocker, D.A. & Laurikainen, E. 1999, AJ, 117, 792
Sandage, A.& Bedke,J. 1994, The Carnegie Atlas of Galaxies. Volume II, Carnegie Institution of Washington with The Flintridge Foundation
Skrutsie, M.F., Cutri, R.M., Stiening, R., Weinberg, M.N., Schneider, S., Carpenter, J.M. et al. 2006, AJ, 131, 1163
ofue, Y. & Rubin, V. 2001, ARA&A, 39, 137
Struck, C. 2005, astro-ph/0511335
Tully, R.B., Verheijen, M.A.W., Pierce, M.J., Huang, J.-S. & Wainscoat, R. J. 1996, AJ, 112, 2471
de Vaucouleurs G., de Vaucouleurs A., Corwin H.G., Buta R.J., Paturel G. &Fouque P. 1991, Third Reference Catalogue of Bright Galaxies (RC3), Springer-Verlag: New York
Verheijen, M.A.W. & Sancisi, R. 2001, A&A, 370, 765
Verheijen, M.A.W. 2001, ApJ, 563, 694

Table 1. Parameters of NGC 3893 and NGC 3896

	NGC 3893	NGC 3896
Coordinates (J2000)[a]	$\alpha = 11h\ 48m\ 38.38$	$\alpha = 11h\ 48m\ 56.42s$
	$\delta = +48^\circ\ 42'\ 34.4''$	$\delta = +48^\circ\ 40'\ 29.2''$
Morphological type	SABc[a]	S0-a[a]
	SAB(rs)c[b,c]	S0/a[c]: pec[b]
	Sc[d]	SBbc pec[d]
m_B[d] (mag)	11.13	14.05
$B - V$[d] (in mag)	0.56	0.46
$D_{25}/2$[a] ($'$)	2.03	0.75
Distance[e] (Mpc)	18.6	18.6
SFR[f] ($M_\odot/yr$)	5.62	0.14
Heliocentric systemic velocity (km/s)	969 ± 3[a,g]	959 ± 12[a,g]
	973[j]	- - -
	962.0 ± 5[h]	920 ± 5[h]
	958.0[k]	- - -
V_{rotmax} (km/s)	251.2[a,g]	150[a,g]
	195[j]	$confused$[j]
	220 ± 3[l]	- - -
	197 ± 10[h]	50 ± 10[h]
	207[k]	- - -
P.A. ($^\circ$)	352[j]	- - -
	$166 + 180$[m]	- - -
	340 ± 10[h]	294 ± 5[h]
	$167 + 180$[k]	- - -
Inclination ($^\circ$)	49 ± 2[i]	48 ± 3[i]
	42[m]	- - -
	45 ± 3[h]	49 ± 3[h]
	49[k]	- - -
m_K[n] (mag)	7.891	11.648

[a] LEDA database
[b] NED database
[c] RC3 (de Vaucouleurs et al.(1991)
[d] Hernández-Toledo & Puerari (2001)
[e] Tully & Pierce (2000)
[f] James *et al* (2004), total measured $H\alpha$ + [NII] line flux corrected for [NII] contamination
[g] From HI observations
[h] This work
[i] Verheijen (2001), HI observations
[j] Verheijen & Sancisi (2001), HI observations
[k] Garrido et al. (2002)
[l] Tully et al.(1996)
[m] Kranz, Slyz & Rix (2003)
[n] 2MASS (Skrutskie et al. 2006) K_{ext} value taken from the NED database

Table 2. Mass models parameters for NGC 3893 from best fits of the multi-wavelength rotation curve considering only points associated to circular motions

Type of halo	Maximal disc	$(M/L)_{disc}$ (I band)	R_0 (kpc)	ρ_0 ($M_\odot/pc^{-3}$)	χ^2
Multi-wavelength curve, non-circular motions excluded					
p-ISO	no	0.940	1.570	0.340	1.34
p-ISO	yes	1.250	2.000	0.210	1.53
NFW	no	0.240	7.160	0.075	1.43
NFW	yes	1.250	7.100	0.050	2.60
Multi-wavelength curve, non-circular motions included					
p-ISO	no	1.050	1.100	0.710	2.16
p-ISO	yes	1.250	1.500	0.310	1.83
NFW	no	0.070	4.650	0.160	1.72
NFW	yes	1.250	7.100	0.050	2.60
Hα curve, non-circular motions included					
p-ISO	no	0.560	1.090	0.900	1.09
NFW	no	0.560	10.100	0.040	0.96
HI curve, non-circular motions excluded					
p-ISO	yes	1.750	2.600	0.079	1.32
NFW	yes	1.745	7.000	0.030	3.17

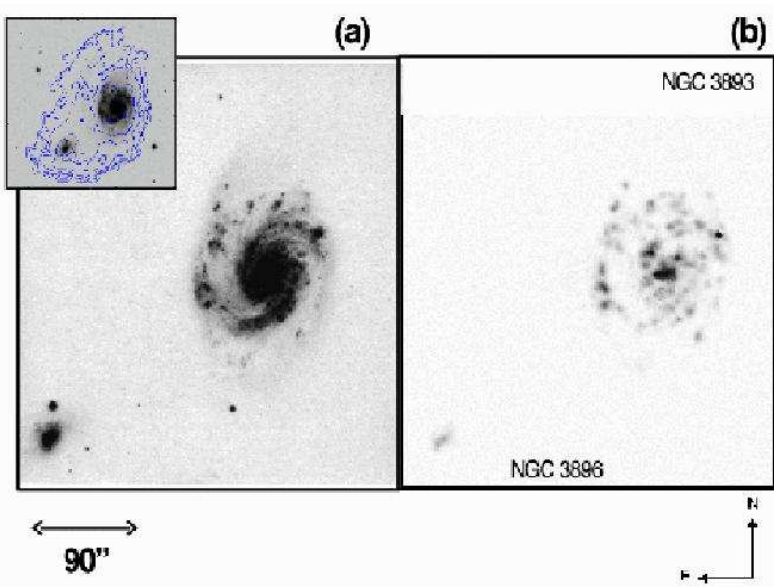

Fig. 1. *a)* Direct B image of NGC 3893/96 (KPG 302) from "The Carnegie Atlas of Galaxies. Volume II" (Sandage & Bedke 1994). *b)* Monochromatic *Hα* (continuum substracted) image of the pair obtained from the scanning Fabry-Perot interferometer PUMA data cubes. *Upper panel:* Optical image with HI isophotes superposed. Image taken from Verheijen & Sancisi (2001) in "An HI Rogues Gallery" *(http://www.nrao.edu/astrores/HIrogues/webGallery/RoguesGallery06.html)*

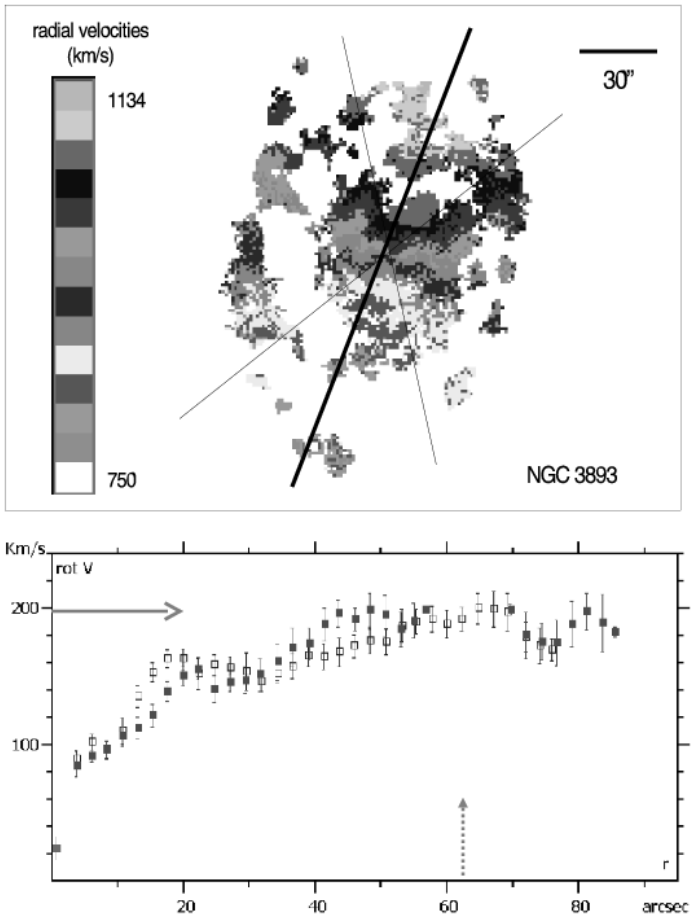

Fig. 2. *Top:* Velocity field of NGC 3893 in KPG 302. Solid line indicates the galaxy's position angle (*P.A.*), slash-dotted lines indicate the angular sectors from both sides of the major axis considered for the computation of the galaxy's the computation of the galaxy's rotation curve. *Bottom:* Rotation curve (RC) of NGC 3893. Both sides of the curve have been superposed. Open squares correspond to the receding side of the galaxy. Filled squares correspond to the approaching side. RC was plotted considering an inclination value of 45°. Horizontal solid arrow indicates the maximal rotation velocity. Vertical dotted arrow indicates the radius associated with corotation according to Kranz, Slyz & Rix (2003).

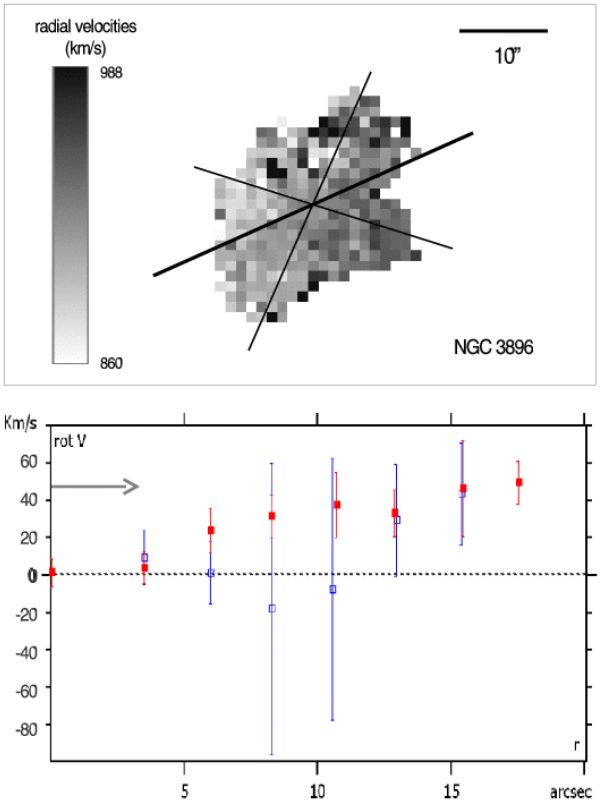

Fig. 3. *Top:* Velocity field of NGC 3896 in KPG302. Solid line indicates the galaxy's position angle (*P.A.*), slash-dotted lines indicate the angular sectors from both sides of the major axis considered for the computation of the galaxy's RC. *Bottom:* RC of NGC 3893. Both sides of the curve have been superposed. Open squares correspond to the receding side of the galaxy. Filled squares correspond to the approaching side. RC was plotted considering an inclination value of 49°. Solid arrow indicates maximal rotation velocity.

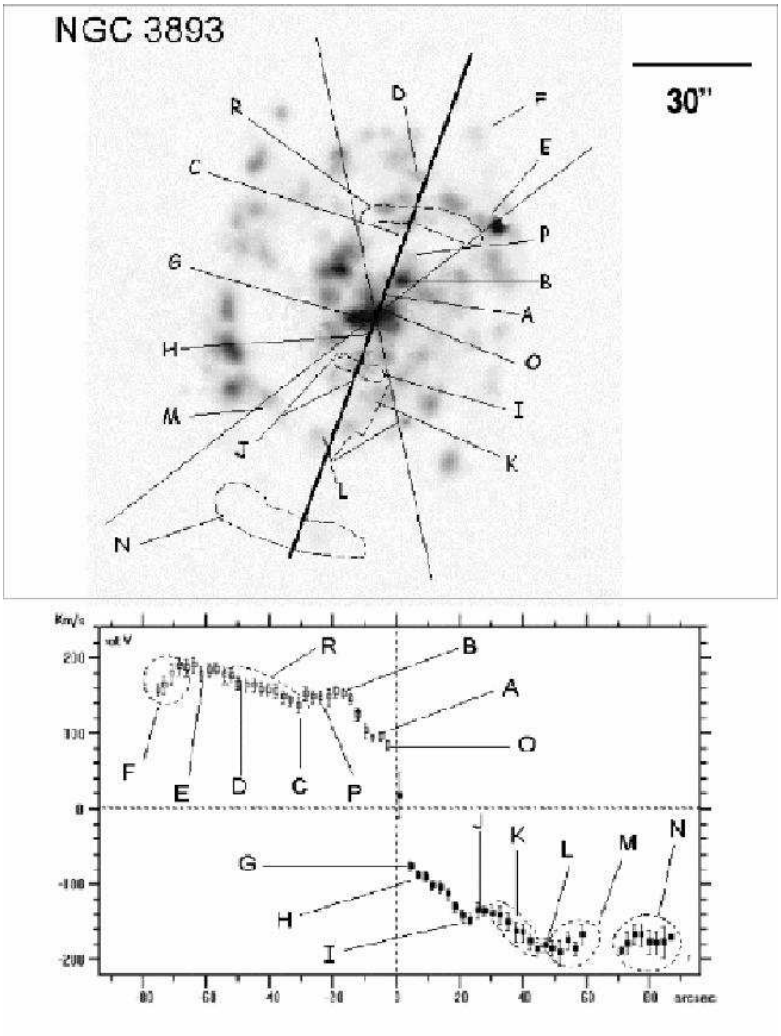

Fig. 4. Top: Monochromatic image of NGC 3893. Letters indicate features associated to points on the RC (shown in the bottom panel) in order to differentiate the contribution of circular from non-circular motions. Solid line indicates the galaxy's position angle (*P.A.*), the thin lines indicate the angular sector from both sides of the major axis considered for the computation of the galaxy's RC.

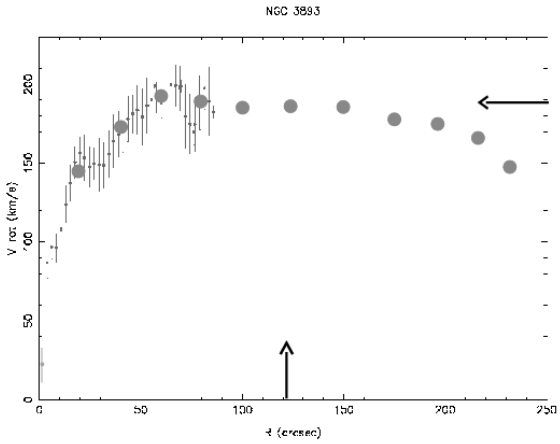

Fig. 5. Multi-wavelength curve of NGC 3893. Small dots in the inner parts of the curve correspond to optical Fabry-Perot $H\alpha$ observations. Larger dots in the outer parts correspond to the HI curve derived by Verheijen & Sancisi (2001). The horizontal arrow indicates the point with maximum rotation velocity. Vertical arrow shows the radius considered for mass estimation using the method by Lequeux (1983).

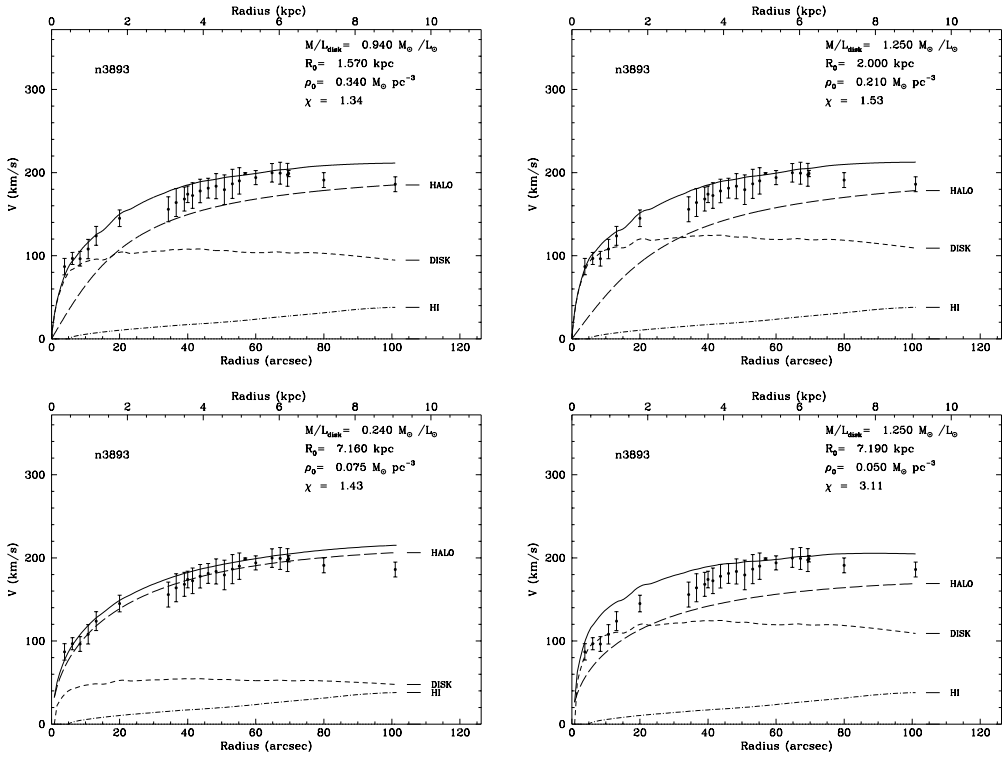

Fig. 6. Best mass model fits for the multi-wavelength rotation curve of NGC 3893 once the points associated with non-circular motions have been removed. *Top left:* Pseudo-isothermal halo and non-maximal disc. *Top right:* Pseudo-isothermal halo and maximal disc. *Bottom left:* NFW halo and non-maximal disc. *Bottom right:* NFW halo and maximal disc. Long-dashed curve represents the dark-matter halo contribution, short-dashed curve represents the stellar disc contribution. The parameters displayed stand for the mass-to-light ration of the stellar disc (M/L_{disc}), the characteristic radius of the dark matter halo and density (R_0 and ρ_0, respectively) and the minimized χ^2 in the three-dimensional parameter space. Mass-model taken from Blais-Ouellette, Amram & Carignan (2001).

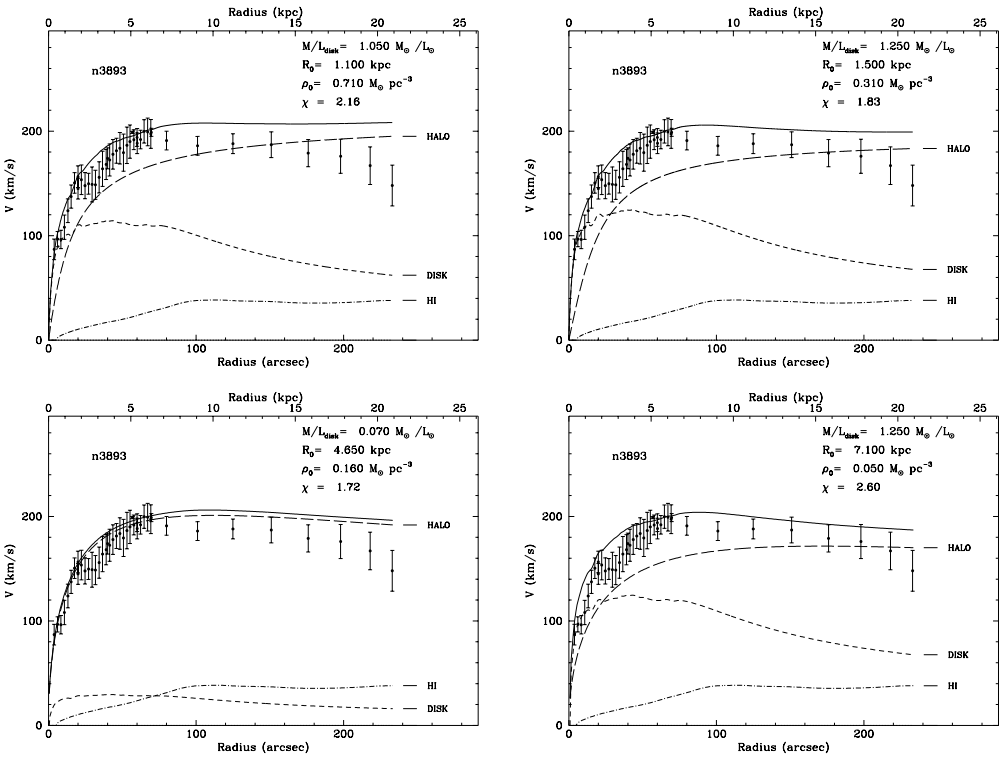

Fig. 7. Best mass model fit for the multi-wavelength rotation curve of NGC 3893 considering all observed points - including those associated with non-circular motions. *Top left:* Pseudo-isothermal halo and non-maximal disc. *Top right:* Pseudo-isothermal halo and maximal disc. *Bottom left:* NFW halo and non-maximal disc. *Bottom right:* NFW halo and maximal disc.

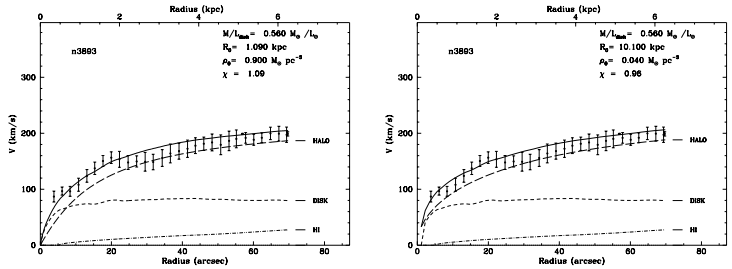

Fig. 8. Best mass model fit for the Hα rotation curve of NGC 3893 considering all observed points -including those associated with non-circular motions and using the $(M\text{Ł})_{disc}$ value by Kranz, Slyz & Rix (2003) . *Left:* Pseudo-isothermal halo. *Right:* NFW halo.

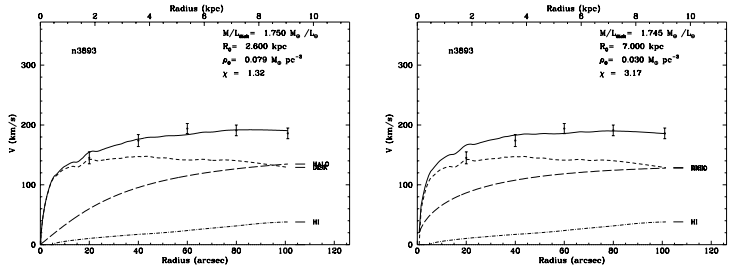

Fig. 9. Best mass model fit for the HI rotation curve of NGC 3893 after removing points associated with non-circular motions and the warp of the outer parts of the disc. *Left:* Pseudo-isothermal halo. *Right:* NFW halo.